Engineering Structures 86 (2015) 72–83

Contents lists available at ScienceDirect

Engineering Structures

journal homepage: www.elsevier.com/locate/engstruct

New finite element to model bond–slip with steel strain effect for the analysis of reinforced concrete structures

José Santos [a,c,*], António Abel Henriques [b,c]

[a] UMa – University of Madeira, CCCEE – Competence Centre of Exact Sciences and Engineering, 9020-105 Funchal, Portugal
[b] FEUP – Faculty of Engineering of the University of Porto, DEC – Department of Civil Engineering, 4200-465 Porto, Portugal
[c] LABEST – Laboratory for the Concrete Technology and Structural Behaviour, Portugal

ARTICLE INFO

Article history:
Received 9 August 2014
Revised 6 December 2014
Accepted 17 December 2014
Available online 10 January 2015

Keywords:
Finite element
Cracking
Reinforced concrete
Bond–slip
Steel strain effect

ABSTRACT

The influence of steel strain in bond–slip relationship has been the subject of recent literature, especially steel strain after yielding. This paper presents a new bond element for finite element packages which performs the bond–slip relationship, including steel strain effect. The developed element consists of an orthotropic four-node plane stress element whose constitutive material laws were changed. In order to verify the accuracy of this element several 2D numerical results were compared with experimental data. The results obtained with this element showed the need for its use to achieve good results and the relevance of steel strain effect on bond–slip relationship, especially in tension elements.

1. Introduction

The behaviour of reinforced concrete (RC) structures is considerably influenced by bond–slip relationship. On the one hand, bond stress should be high enough to minimise crack width and deformations in service, and, on the other hand, bond stress should be low enough to ensure large rotation capacity at plastic hinges near the failure.

For many years researchers have described bond stress mainly as a function of the slip between steel and concrete. The influence of other parameters was disregarded because numerical and experimental studies were mostly developed in service conditions, that is, before the yield of steel. Many studies are discussed in FIB Bulletin 10 [1]. The most well-known relationship between bond stress and slip is given by Eq. (1), which is used in many codes like Model Code 2010 (MC2010) [2]:

$$\tau_0(s) = \begin{cases} 2.5 \cdot \sqrt{f_c} \cdot s^{0.4}; & 0 \leqslant s \leqslant 1.0 \\ 2.5 \cdot \sqrt{f_c}; & 1.0 < s \leqslant 2.0 \\ \sqrt{f_c} \cdot \left(2.5 - 1.5 \cdot \frac{s-2.0}{c_{clear}-2.0}\right); & 2.0 < s \leqslant c_{clear} \\ \sqrt{f_c}; & s > c_{clear} \end{cases} \quad (1)$$

where f_c = compressive strength of concrete; c_{clear} = clear distance between ribs in the rebar.

More recently, because of the need to ensure ductile behaviour in reinforced concrete structures near the failure, several researchers have proposed extended formulations for bond–slip relationship, which take into account the post-yield tension stiffening effects. Parameters like steel strain, concrete strain, damage or confinement have been related to bond–slip relationship.

First, Shima et al. [3] formulated a constitutive model for bond behaviour which includes a relationship between bond stress, slip and steel strain. This model also includes the effects of bar diameter and concrete strength. By means of experimental data in the post-yield range of steel the model was validated. Eqs. (2–4) summarise this proposal:

$$\tau(f_c, s, \varepsilon_s, \varnothing) = \tau_0(f_c, s, \varnothing) \cdot g(\varepsilon_s) \quad (2)$$

$$\tau_0(f_c, s, \varnothing) = 0.73 \cdot f_c \cdot \left[\ln\left(1 + 5000 \cdot \frac{s}{\varnothing}\right)\right]^3 \quad (3)$$

$$g(\varepsilon_s) = \frac{1}{1 + \varepsilon_s \cdot 10^5} \quad (4)$$

where τ = bond stress, f_c = compressive strength of concrete, s = slip between steel and concrete, ε_s = steel strain, $\varnothing$ = diameter of rebars, τ_0 = reference value of bond stress and $g(\varepsilon_s)$ = reduction function.

* Corresponding author at: UMa – University of Madeira, CCCEE – Competence Centre of Exact Sciences and Engineering, 9020-105 Funchal, Portugal.
E-mail address: jmmns@fe.up.pt (J. Santos).

http://dx.doi.org/10.1016/j.engstruct.2014.12.036
0141-0296/

Marti et al. [4] presented the Tension Chord Model, which can be applied in problems of cracking, minimum reinforcement, tension stiffening and rotation capacity. This model assumes a rigid-perfectly plastic bond–slip relationship, but when the steel strain on rebar reaches the yield strain, the bond stress drops to half (Eq. (5)):

$$\tau(f_c, \varepsilon_s) = \begin{cases} 0.6 \cdot f_c^{2/3}; & \varepsilon_s \leqslant \varepsilon_y \\ 0.3 \cdot f_c^{2/3}; & \varepsilon_s > \varepsilon_y \end{cases} \quad (5)$$

where ε_y = yield steel strain.

With regard to experimental results Mayer and Eligehausen [5] recognised the need to model bond by taking into account the effect of steel yield and bar surface geometry.

Lundgren and Gylltoft [6] developed a three-dimensional interface element to connect concrete to the rebar. In this interface element the bond stress depends not only on the slip, but also on the radial deformation between the rebar and the concrete. By using this element in a finite element analysis is possible to predict reasonably splitting failures and loss of bond if the rebar is yielding.

Ožbolt et al. [7] presented a discrete two-node bond element which can be used in the 3D finite element analysis of concrete structures. The model response is controlled by a bond–slip relationship modified to include the loading–unloading–reloading, the concrete geometry, the concrete strain and the steel strain (Eq. (6)). This model applies non-local analysis from the vicinity of the rebar.

$$\Omega_s(\varepsilon_s) = \begin{cases} 1.0; & \varepsilon_s < \varepsilon_y \\ 1.0 - \alpha \frac{\varepsilon_s - \varepsilon_y}{\varepsilon_u - \varepsilon_y}; & \varepsilon_y < \varepsilon_s < \varepsilon_u \\ 1.0 - \alpha; & \varepsilon_u < \varepsilon_s \end{cases} \quad (6)$$

where $\Omega_s(\varepsilon_s)$ = reduction function and α = parameter which controls residual stress.

Lowes et al. [8] proposed a bond element whose constitutive model includes a typical bond–slip relationship, but also the effects of concrete confining pressure, concrete damage, steel strain (Eq. (7)) and others specific for cyclic loading. However, this formulation estimates some essential parameters by non-local techniques.

$$\Gamma_2(\varepsilon_s) = \begin{cases} 1.0; & \varepsilon_s < \varepsilon_y \\ 0.1 + 0.9e^{0.4}\left(1 - \frac{\varepsilon_s}{\varepsilon_y}\right); & \varepsilon_s > \varepsilon_y \end{cases} \quad (7)$$

where $\Gamma_2(\varepsilon_s)$ = reduction function.

Ruiz et al. [9] presented two models that describe the pre- and post-yield relationship of bond in reinforced concrete: the Square-Root Model (Eq. (8)) and the Rigid–Plastic Model (Eq. (9)). Besides the slip, the strain and stress of steel are used to calculate the bond stress:

$$k_b(\varepsilon_s) = \frac{\varepsilon_{bu} - \varepsilon_s}{\varepsilon_{bu} - \varepsilon_y} \cdot \sqrt{\frac{\varepsilon_y}{\varepsilon_s}} \quad 0 \leqslant k_b(\varepsilon_s) \leqslant 1 \quad (8)$$

$$k_b(\varepsilon_s) = e^{10 \cdot (\varepsilon_y - \varepsilon_s)} \quad 0 \leqslant k_b(\varepsilon_s) \leqslant 1 \quad (9)$$

where $k_b(\varepsilon_s)$ = reduction function, $\varepsilon_{bu} = 4 \cdot a/\varnothing$ [generally between 0.07 and 0.12] and a = height of the ribs.

Wu and Gilbert [10] proposed a bond–slip relationship based on CEB-FIP Model Code 1990 (MC90) [11], suitably modified to include the effects of concrete damage, steel stress (Eq. (10)) and confinement. These authors implemented their formulation into an existing finite element code by using non-local analysis.

$$\lambda_2(\sigma_s) = \begin{cases} 1.0; & \sigma_s < 250 \text{ MPa} \\ 2.0 - 0.004 \cdot \sigma_s; & 250 \text{ MPa} \leqslant \sigma_s \leqslant 500 \text{ MPa} \\ 0.0; & \sigma_s > 500 \text{ MPa} \end{cases} \quad (10)$$

where $\lambda_2(\sigma_s)$ = reduction function and σ_s = steel stress.

According to MC2010 [2], the bond–slip curve is considerably influenced by reinforcement yielding and transverse pressure. Therefore, MC2010 defines two factors necessary to reduce the value of the bond defined in MC90: the first depends on the steel strain and the ductility of steel (Eq. (11)), and the second depends on the compressive stress (orthogonal to the rebar axis):

$$\Omega_y(\varepsilon_s) = \begin{cases} 1.0; & \varepsilon_s \leqslant \varepsilon_y \\ 1.0 - \left[0.85 \cdot \left(1.0 - e^{-5 \cdot a^b}\right)\right]; & \varepsilon_y \leqslant \varepsilon_s \leqslant \varepsilon_u \end{cases} \quad (11)$$

$$a = \frac{\varepsilon_s - \varepsilon_y}{\varepsilon_u - \varepsilon_y}; \quad b = \left[2.0 - \frac{f_t}{f_y}\right]^2 \quad (12)$$

where $\Omega_y(\varepsilon_s)$ = reduction function, a and b are calculated by Eq. (12).

Lee et al. [12] presented a tension stiffening model which enables the calculation of average tensile stresses in concrete after yielding of steel. This model uses the factor proposed by Ruiz et al. [9] for the influence of steel strain on bond stress. The numerical results indicated good agreement with experimental values including after the yielding of steel.

All cited authors recognise the influence of steel strain on the bond–slip relationship after the yielding of steel. For this reason, its implementation in finite element (FE) models has considerable relevance. The classical models with non-linear springs cannot be applied because only the slip is used. Wu and Gilbert [10] successfully developed and implemented a bond element (including slip and steel strain), but used non-local analysis. To the best of our knowledge, in the literature there are no bond elements which include slip and steel strain in their formulation, without any non-local analysis.

The aim of this paper is to develop a bond element for connecting concrete to steel, which takes into account the steel strain in the bond–slip relationship, without changing the usual organisation of software code.

To achieve this aim: (i) a new bond element was formulated and (ii) several numerical examples were tested by comparing their results with experimental data for different situations regarding reinforced concrete: tension, compression and bending.

The results obtained from the performed analyses showed that the proposed new bond element is capable to simulate satisfactorily the experimental tests.

The results obtained in numerical simulations which use the developed bond element may be used to study many critical problems of reinforced concrete structures, like: crack spacing, minimum reinforcement, tension stiffening, rotation capacity, ductility and deflection. With the steady increase in processing power of computers is expected that modelling tend to more refined and detailed models where the proposed new bond element may be often applied.

2. Formulation of the bond element

The bond element was implemented in Diana software [13], which allows users to define and implement new formulations for materials. In the 'General User-supplied Material Model' only the subroutine USRMAT which computes the matrices respecting to the total stress (σ) and tangent stiffness (D) needs to be defined. The rest of the software code remains unchanged.

Besides the current data (materials and geometry), in each increment this subroutine has as input variables: total strain (ε), total stress (σ), stiffness (D), and incremental strains ($\Delta\varepsilon$), whereas the output variables are only: total stress (σ) and stiffness (D).

The bond element developed in this paper consists of an orthotropic four-node plane stress element, whose constitutive material laws were changed to perform the bond–slip relationship.

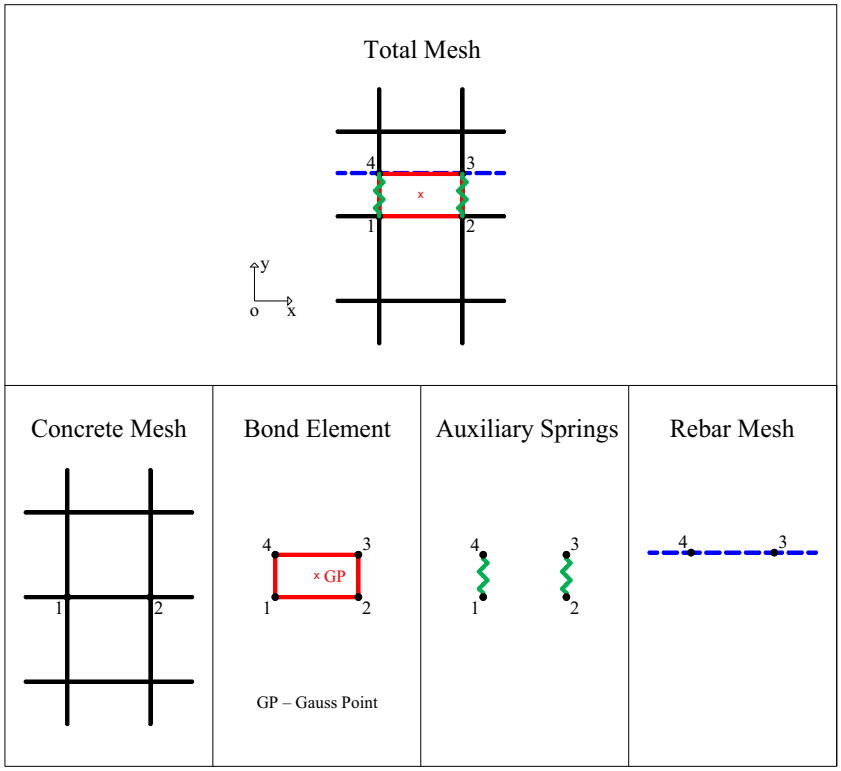

Fig. 1. Connection between concrete and rebar.

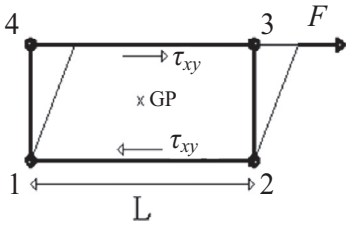

Fig. 2. Shear stress (τ_{xy}) in element.

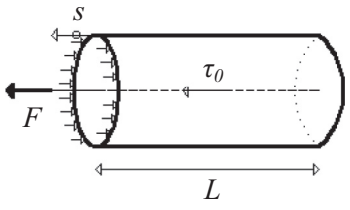

Fig. 3. Pull-out test.

The influence of steel strain can be included by taking into account the assumptions described in the following paragraphs. Although this element has been applied with other plane stress elements (2D), it can be applied with solid elements (3D). The rebar is simulated with truss elements and the concrete with plane stress elements.

Fig. 1 shows the connection between the concrete and rebar created by the bond element. The bond element connects with concrete in nodes 1 and 2 and with the rebar in nodes 3 and 4. Simply, the shear stress (τ_{xy}) is related to bond stress (τ_0) and the shear strain (γ_{xy}) to slip (s). To avoid shear strains that are not related to slip, auxiliary springs with (theoretical) infinite stiffness are used to connect nodes 1 & 4 and nodes 2 & 3. To simplify the problem and to describe the formulation easily only one integration point was used for this element (GP in Figs. 1, 2, 5 and 6).

First of all, the total stress (σ) and tangent stiffness (D) are calculated with Eqs. (13) and (14). In the total stress vector, the first components (σ_{xx} and σ_{yy}) are zero in order to avoid incorrect stresses in the structure, and third component (τ_{xy}) gives the bond:

$$\sigma = \begin{bmatrix} 0 \\ 0 \\ \tau_{xy}(s, \varepsilon_s) \end{bmatrix} \tag{13}$$

where s = slip; ε_s = steel strain; and τ_{xy} = shear strain.

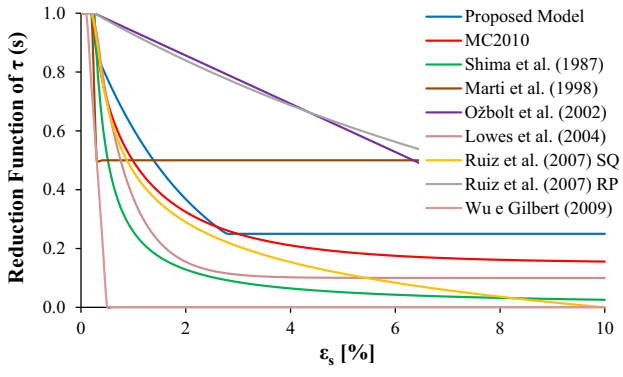

Fig. 4. Comparison of reduction function.

In tangent stiffness all directions are independent (Poisson's ratio is equal to zero), and their values are derived from total stress, except the elements k_{11} and k_{22} for numerical reasons:

$$D = \begin{bmatrix} 1 & 0 & 0 \\ 0 & 1 & 0 \\ 0 & 0 & \frac{d\tau_{xy}(s,\varepsilon_s)}{d\gamma_{xy}} \end{bmatrix} \tag{14}$$

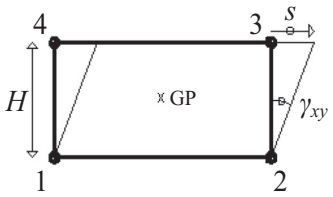

Fig. 5. Estimation of slip (s).

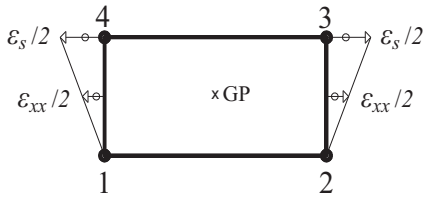

Fig. 6. Estimation of steel strain (ε_s).

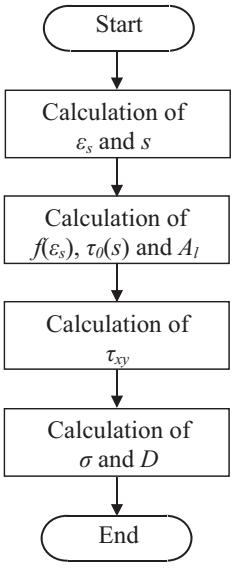

Fig. 7. Subroutine flowchart.

Inside the subroutine USRMAT only the element strains are available (ε_{xx}, ε_{yy}, γ_{xy}), so the values of slip (s) and steel strain (ε_s) are estimated from the element strains: ε_{xx} and γ_{xy} respectively. Thus, Eqs. (13) and (14) are replaced by Eqs. (15) and (16), now totally formulated from the element strains:

$$\sigma = \begin{bmatrix} 0 \\ 0 \\ \tau_{xy}\left(\varepsilon_{xx}, \gamma_{xy}\right) \end{bmatrix} \tag{15}$$

$$D = \begin{bmatrix} 1 & 0 & 0 \\ 0 & 1 & 0 \\ 0 & 0 & \frac{d\tau_{xy}(\varepsilon_{xx},\gamma_{xy})}{d\gamma_{xy}} \end{bmatrix} \tag{16}$$

where ε_{xx} = strain according to the rebar direction and γ_{xy} = shear strain.

In Fig. 2 a uniform force is applied to the rebar (note that the configuration of the deformed element is only valid because auxiliary springs were used). Therefore, the shear stress (τ_{xy}) in the element can be calculated from force (F), length (L) and width (b) of the element, as in Eq. (17):

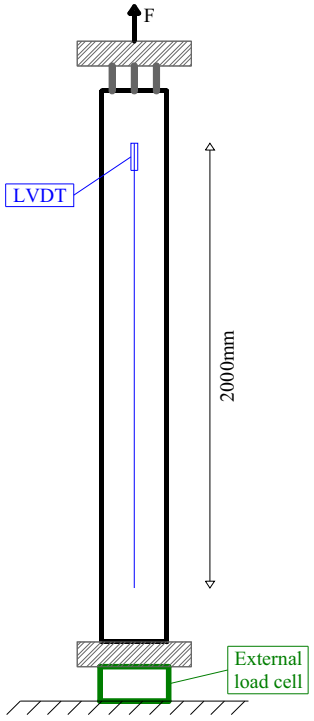

Fig. 8. Test set-up of the tensile tests.

Table 1
Geometry and reinforcement of ties.

Designation	ρ (%)	Dimensions (m)
4∅12	0.50	0.30 × 0.30 × 2.50
4∅16	0.50	0.40 × 0.40 × 2.70
8∅12	1.00	0.30 × 0.30 × 2.50
8∅16	1.00	0.40 × 0.40 × 2.70

$$\tau_{xy} = \frac{F}{b \cdot L} \tag{17}$$

Fig. 3 shows a pull-out test, where the bond–slip relationship is usually measured. The bond stress (τ_0) can be calculated from force (F), length (L) and perimeter (A_l) of the rebars, according to Eq. (18). The perimeter (A_l) can be computed from Eq. (19):

$$\tau_0 = \frac{F}{L \cdot A_l} \tag{18}$$

$$A_l = \pi \cdot n \cdot \varnothing \tag{19}$$

where n = number of rebars; and $\varnothing$ = diameter of rebars.

From Eqs. (17) and (18) the shear stress (τ_{xy}) can be obtained as a function of bond stress (τ_0), width (b) and perimeter (A_l), as shown in Eq. (20). To simplify, width is assumed to be unitary, resulting in Eq. (21). This is a relevant equation in this paper because it relates the shear stress (τ_{xy}) in the finite element to the bond stress (τ_0) in the concrete:

$$\tau_{xy} = \tau_0 \cdot \frac{A_l}{b} \tag{20}$$

$$\tau_{xy} = \tau_0 \cdot A_l, \text{ for } b = 1 \tag{21}$$

So far the basic expressions for total stress (σ) and tangent stiffness (D) have been introduced. In these expressions only the bond stress (τ_0) is a function of slip (s) and steel strain (ε_s), and the other

parameters are constant in each step. In the next paragraphs the detail of these parameters (τ_0, s and ε_s) is presented.

In Eq. (20), apart from the introduction of slip (s) and steel strain (ε_s), a division of this equation into two terms is now considered. Depending on whether the steel strain (ε_s) level in the rebar is higher or lower than the yield steel strain (ε_y), a different option is chosen. According to Eq. (22), when $\varepsilon_s \leqslant \varepsilon_y$ a current bond–slip relationship is applied, but when $\varepsilon_s > \varepsilon_y$ the value of τ_0 is fixed and a new factor $f(\varepsilon_s)$ depending only on the steel strain controls the bond:

$$\tau_{xy}(s,\varepsilon_s) = \begin{cases} \tau_0(s)\cdot A_l; & 0 \leqslant \varepsilon_s \leqslant \varepsilon_y \\ \tau_0(s_{\varepsilon_y})\cdot A_l \cdot f(\varepsilon_s); & \varepsilon_s > \varepsilon_y \end{cases} \tag{22}$$

where s_{ε_y} = slip at the instant of first yield and $f(\varepsilon_s)$ = a reduction function of bond stress.

This second term is different from the expression of MC2010 [2] in Eq. (23). Note that although the $f(\varepsilon_s)$ and $\Omega_y(\varepsilon_s)$ are very similar functions, the second term of Eq. (22) fixes the value of τ_0, unlike the expression of MC2010. In Section 3, the results of two models are compared.

$$\tau_{xy}(s,\varepsilon_s) = \tau_0(s)\cdot A_l \cdot \Omega_y(\varepsilon_s) \tag{23}$$

The bond–slip relationship $\tau_0(s)$ chosen for this paper was the expression proposed by MC2010 because it reproduces the pull-out tests very well. This expression is shown in Eq. (1).

The function $f(\varepsilon_s)$ was previously calibrated from experimental results described in the literature, namely the ties tested by Mayer and Eligehausen [5]. This function is shown in Eq. (24).

$$f(\varepsilon_s) = \begin{cases} 1.0; & 0 \leqslant \varepsilon_s \leqslant \varepsilon_y \\ e^{-50\cdot\varepsilon_s} \geqslant 0.25; & \varepsilon_s \geqslant \varepsilon_y \end{cases} \tag{24}$$

The calibration process consisted in the trial and error method: (i) the four ties referred in Section 3.1 were calculated for several reduction functions, (ii) the function which best fit all the results were selected, (iii) the four ties were calculate again for several values of the previous selected function, and (iv) the values which best fit all the results were selected.

When the calibration process started it was also noted the need to fix the value of τ_0 after the yielding, as previously mentioned. This happened because if τ_0 was not fixed, the function $\tau_0(s)$ increased faster than the reduction of the function $f(\varepsilon_s)$, nullifying the anticipated reduction in $\tau_{xy}(s,\varepsilon_s)$. This fact is physically controversial; however it can be defensible by the fact that as these rebars have a large yield plateau, when they restart increasing stress after the plateau, they have reduced so much their diameter that it can be assumed the bond stress cannot increase anymore.

In Fig. 4 the function $f(\varepsilon_s)$ is compared with similar functions available in the literature to reduce $\tau_0(s)$. In this simulation the following parameters were assumed for steel: ε_y = 2.5‰, ε_u = 100‰, f_y = 550 MPa and f_t = 650 MPa. Although not all curves are directly comparable, because some of them are associated with different expressions for $\tau_0(s)$, it is possible to find some similarities between them.

Finally, in the next paragraphs the slip (s) and steel strain (ε_s) are deduced from the bond element strains.

In Fig. 5 a uniform slip is introduced into the rebar. As a result, the slip (s) can be calculated from the shear strain (γ_{xy}) and height of element (H), according to Eq. (25):

$$s \approx \gamma_{xy}\cdot H \tag{25}$$

In Fig. 6 a uniform strain is introduced into the rebar so the steel strain (ε_s) can be estimated from strain according to the x-axis (ε_{xx}), as shown in Eq. (26):

$$\varepsilon \approx 2\cdot\varepsilon_{xx} \tag{26}$$

To develop Eqs. (25) and (26) the concrete strain was assumed to be zero, which is not strictly true. Nevertheless, in the cracked concrete the steel strain is much higher than concrete strain, especially near the cracks, so the simplification applied is acceptable.

Fig. 7 shows the calculation flowchart used in the subroutine USRMAT to calculate the total stress (σ) and stiffness (D) matrices. In all numeric examples developed in this paper the following conditions were used: (i) for bond element a ratio H/L = 0.10 and (ii) for auxiliary springs a stiffness $K = 10^{15}$ N/m.

3. Comparison with experimental data

In order to assess the applicability of the developed bond element some comparisons with experimental data were carried out. To cover likely situations arising in reinforced concrete three cases were selected: (i) tension, (ii) compression, and (iii) bending. In all cases the steel strain was higher than the yield strain.

3.1. Tensile tests in ties

Mayer and Eligehausen [5] tested several reinforced concrete ties up to failure. Note that the reduction function $f(\varepsilon_s)$ was previously calibrated by trying to simulate some of these ties. These tests were chosen for the calibration because: (i) they are representative of the knowledge in the literature; (ii) they are in pure tension; and (iii) their results are global (average of several cracks).

3.1.1. Test set-up

Fig. 8 shows the test set-up, and Table 1 details the geometry and reinforcement of specimens chosen for this comparison. Four ties were selected to typify current situations in reinforced concrete: rebar diameter of 12 and 16 mm, and reinforcement ratio of 0.5% and 1.0%.

3.1.2. Numeric model

To simulate these ties numeric models with finite elements in plane stress state were developed. Fig. 9a shows the major elements of finite element mesh, the supports and loading for ties with ρ = 0.50%. The major elements refer to the initial elements of each material which were further divided into smaller elements. The connection between concrete, bond elements and rebars was similar to that in Fig. 1.

Concrete was simulated by regular four-node plane stress elements, with dimensions of 0.01×0.01 m^2 and an integration scheme of 2×2 Gauss points. Compression rebars and stirrups were simulated by embedded bar reinforcements. The rebars and the bond element were simulated as presented in Section 2, with dimensions of 0.01×0.001 m^2 (bond), and 0.01 m (rebar) and an integration scheme of 1×1 Gauss points.

The loading process was implemented by displacement increments. The BFGS (a Quasi-Newton method) was chosen as solution algorithm [13]. Three norms (force, energy and displacements) were used as convergence criteria. Line search algorithms were also used to increase the convergence rate.

The properties of materials took into account non-linear behaviour. Isotropic plasticity by Von Mises model was used for steel rebars. For concrete elements the combination of Rankine Principal Stress (in tension) with Drucker–Prager (in compression) was selected to avoid: (i) incoherences in mesh deformation after cracking (namely, unrealistic low strain perpendicular to the cracks because of the Poisson effect) in the Total Strain Models, and (ii) unrealistic constant value for shear retention, which is needed in the Multi-Directional Fixed Crack Model [13,14].

For non-linear tension behaviour, the Hordijk curve for tension softening with G_f (fracture energy) given by the expression of

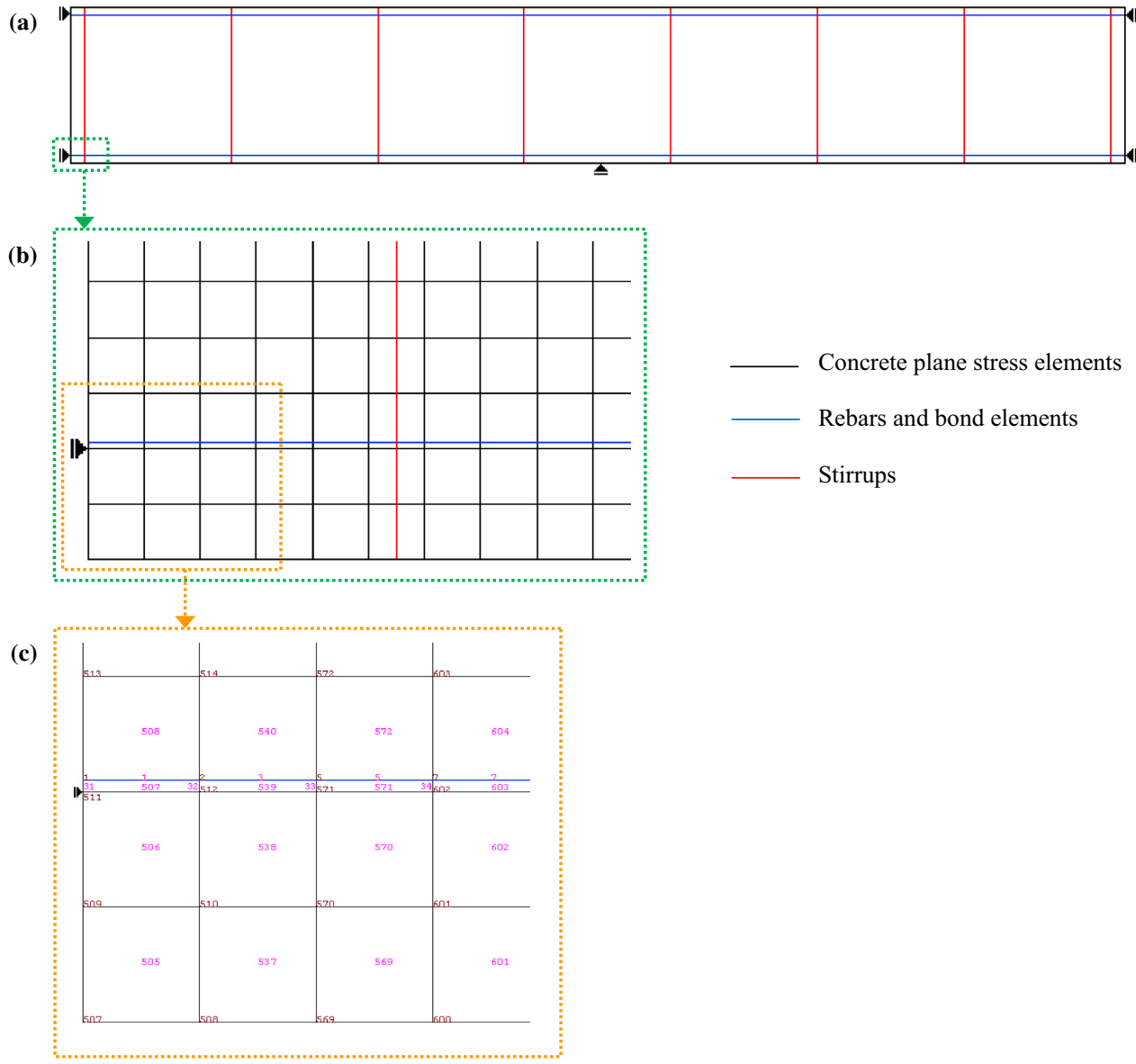

Fig. 9. Finite element mesh for tension test: (a) major elements, (b) detail of the total mesh, (c) multi-detailed mesh with element and node numbers.

MC2010 [2] was applied. For non-linear compression behaviour, the Drucker-Prager law of isotropic plasticity with a parabolic curve for strain hardening was chosen. The values for the material properties were selected exactly in line what was reported in literature.

3.1.3. Results

Fig. 10 shows the results for each tie with the curves of the ratios between mean steel strain (ε_{sm}) and steel strain at the crack (ε_{sr}) as a function of steel strain at the crack (ε_{sr}). Note that the bond element proposed can be used both when the steel strain effect is taken into account (curves 'Proposed Model' and 'MC2010') and when it is not (curve 'MC90'), simply by disabling the reduction factor. Therefore, the base results are represented by curve 'MC90', which only takes into account the function $\tau_0(s)$ (Eq. (1)), whereas the steel strain effect is achieved by adding the function $f(\varepsilon_s)$ (Eq. (24)) in the case of 'Proposed Model', or the function $\Omega_y(\varepsilon_s)$ (Eq. (11)) in the case of 'MC2010'.

The results suggest that in tension elements the effect of steel strain in bond is essential to achieve good global and local results, especially after the yielding of steel. Note also that the results of the proposed model fitted better with experimental data than the results of MC2010. A trend towards the increase of mean steel strain with the increase of rebar diameter and/or the amount of reinforcement was also noted. This aspect was adequately simulated by the proposed model.

Fig. 11 shows the numerical crack patterns for all ties with the proposed model. Small changes occur if the reduction function of MC2010 or MC90 is used. The influence of rebar diameter and reinforcement ratio is clearly exhibited in these results: (i) the larger the diameter, the greater the crack spacing; (ii) the larger the reinforcement ratio, the smaller the crack spacing. As expected the crack spacing is almost constant, especially for specimen with high reinforcement ratio.

3.2. Pull-out tests

Pull-out tests are usually performed to obtain the curve $\tau_0(s)$, and for this reason much information is available in the literature about bond stress, steel strain and slip. It is important to remember

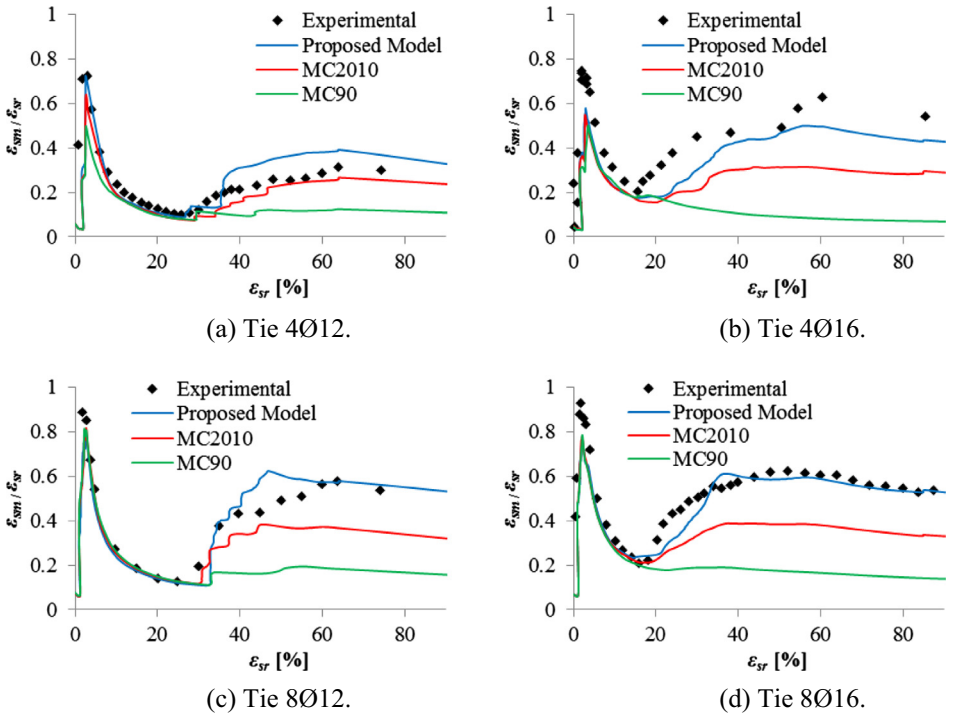

Fig. 10. Tensile tests: numerical vs experimental.

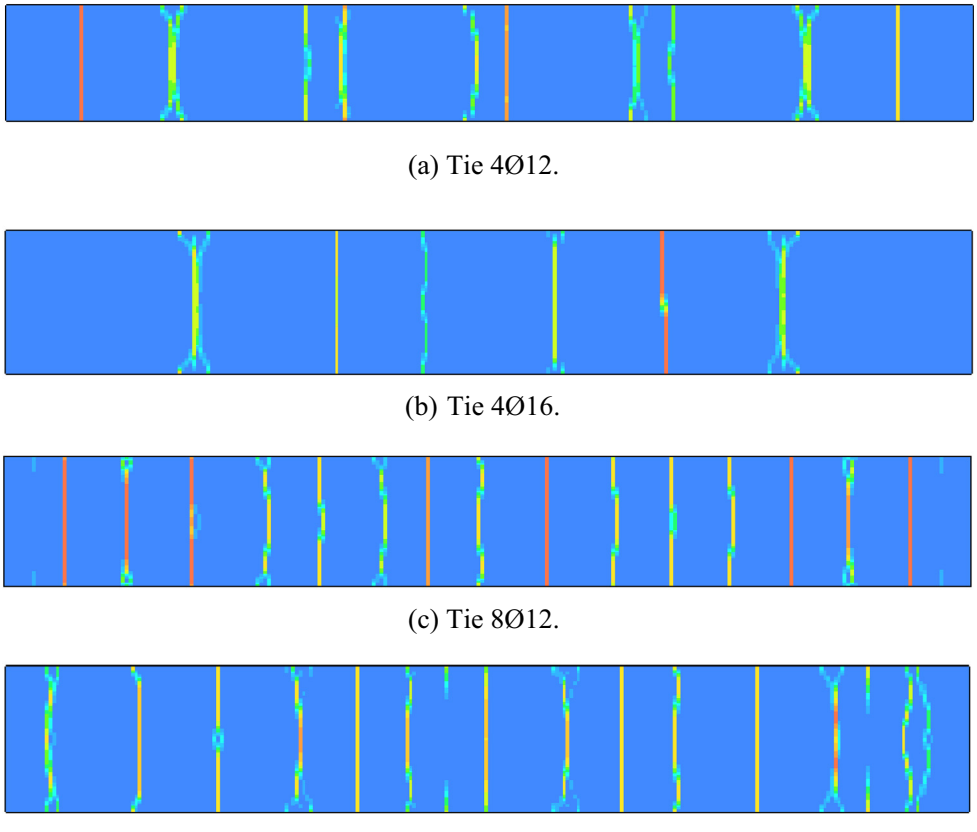

Fig. 11. Crack patterns.

that during these tests the concrete is in compression, so it shows no cracking. Although the steel strain clearly exceeds the yield strain, the function $f(\varepsilon_s)$ was calibrated to a situation of cracked concrete and therefore it is important to assess the applicability of the proposed model to the situation of non-cracked concrete.

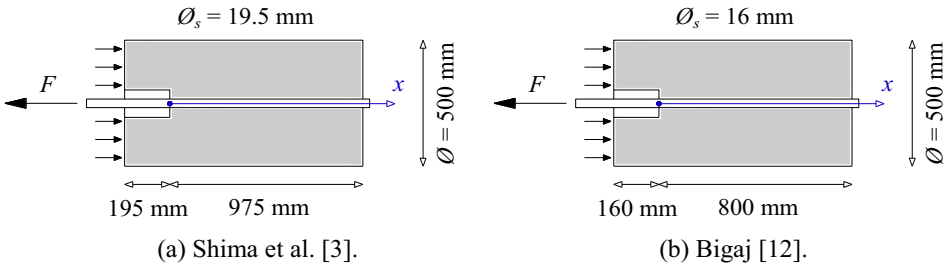

(a) Shima et al. [3]. (b) Bigaj [12].

Fig. 12. Specimen dimensions of the pull-out test.

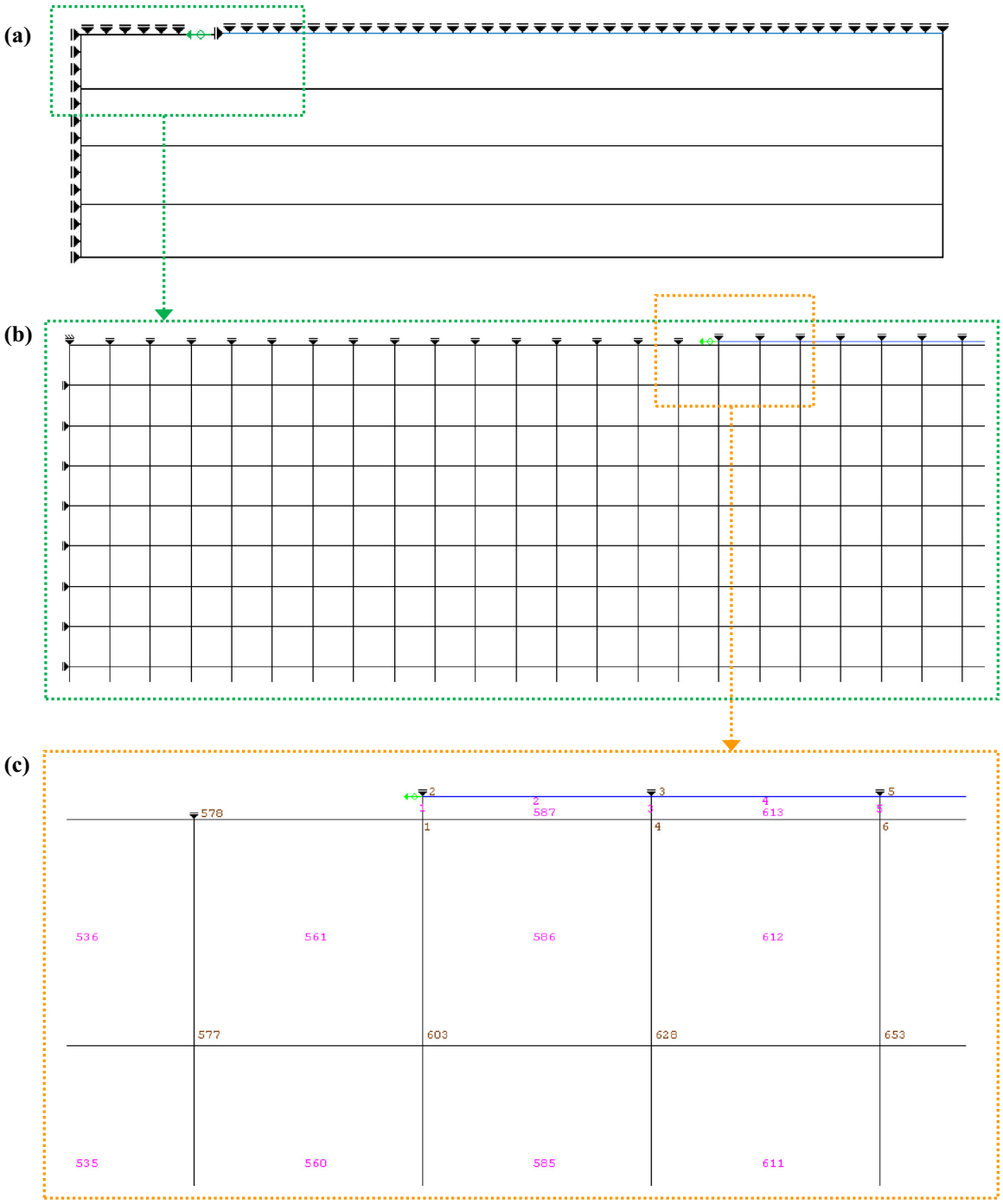

Fig. 13. Finite element mesh for pull-out tests: (a) major elements, (b) detail of the total mesh, (c) multi-detailed mesh with element and node numbers.

3.2.1. Test set-up

Two pull-out tests were selected from the literature: (i) the first from Shima et al. [3], and (ii) the second from Bigaj [15]. The set-ups of the two tests are similar (Fig. 12), although they differ slightly in the rebar diameter and consequently in the bond length. The rebar of Shima et al. [3] had a yield stress higher than 820 MPa and a strain at maximum force of 4.5%, whereas that of Bigaj [15] had a yield stress of 540 MPa and a strain at maximum force of 11.5%.

3.2.2. Numeric model

Fig. 13 shows the major elements of finite element mesh, the supports and loading for the first test. Given the horizontal symmetry of the tests, only half of the specimens were simulated. To this end, vertical supports were introduced in the symmetry axis to restrict the vertical displacements, and the cross-section area of the rebar and the perimeter (A_l) were reduced by half. As the specimens were cylindrical and the elements of mesh were plane stress elements, the concrete mesh was divided into four zones, each with a different thickness. Values for the mechanical properties of materials included in the numeric model were those cited by the authors of the tests, and all other parameters were identical to those described in Section 3.1.2.

3.2.3. Results

Figs. 14–16 compare the results obtained for the bond stress, the steel strain and the slip along the depth of the rebar. Generally, the models which take into account the effects of steel strain in bond showed much better results than the base model ('MC90'). The initial part of the curve of bond stress for the 'Proposed Model', when the steel strain is high, diverged from the 'Experimental Curve' in the case of Bigaj. However, even with the base model ('MC90') it was not possible to obtain an accurate curve. Nevertheless, in the test of Shima et al. the 'Proposed Model' exhibited interesting results.

Regarding steel strain, the 'Proposed Model' showed results similar to the 'Experimental' data with the exception of the region of the yield plateau. In that region the steel strains were lower than the values obtained by Shima et al., but higher than those of Bigaj. In turn, in the two tests the 'MC2010' curve exhibited strains lower

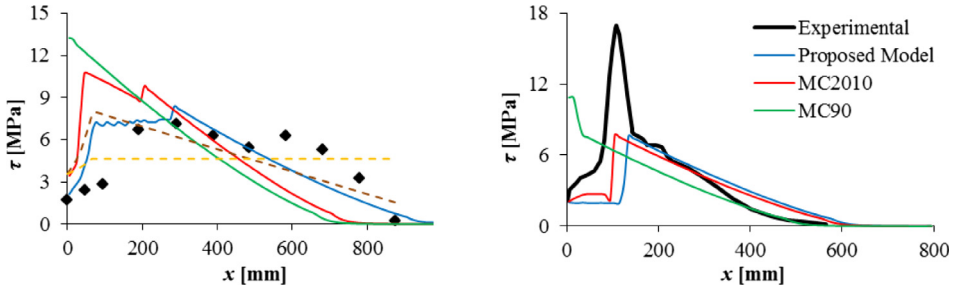

(a) Test SD70 [3]. (b) Test P.16.16.1 [12].

Fig. 14. Pull-out tests: bond stress.

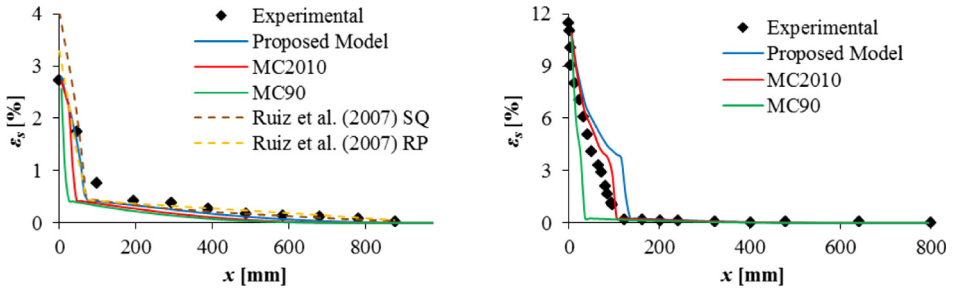

(a) Test SD70 [3]. (b) Test P.16.16.1 [12].

Fig. 15. Pull-out tests: steel strain.

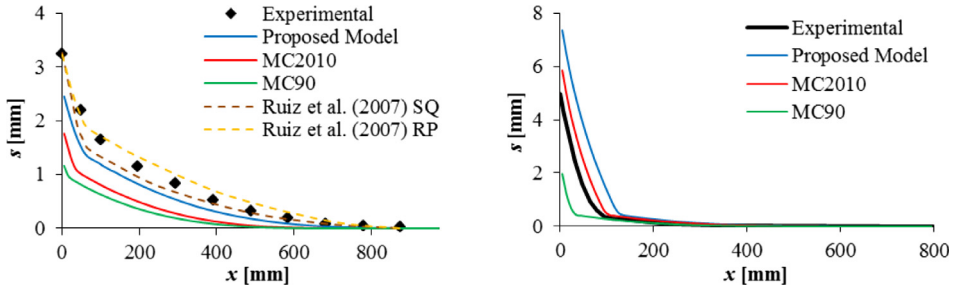

(a) Test SD70 [3]. (b) Test P.16.16.1 [12].

Fig. 16. Pull-out tests: slip.

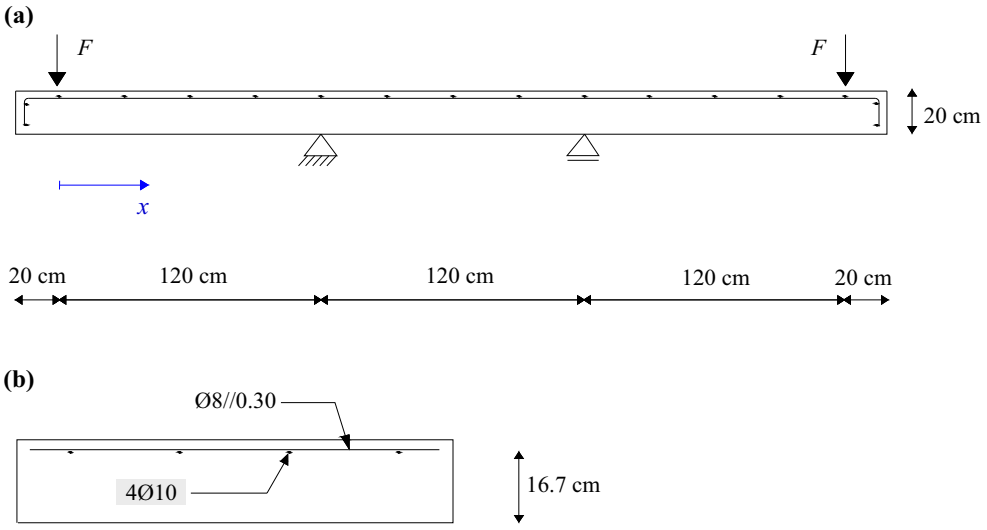

Fig. 17. Test set-up of the bending test: (a) elevation, (b) cross-section.

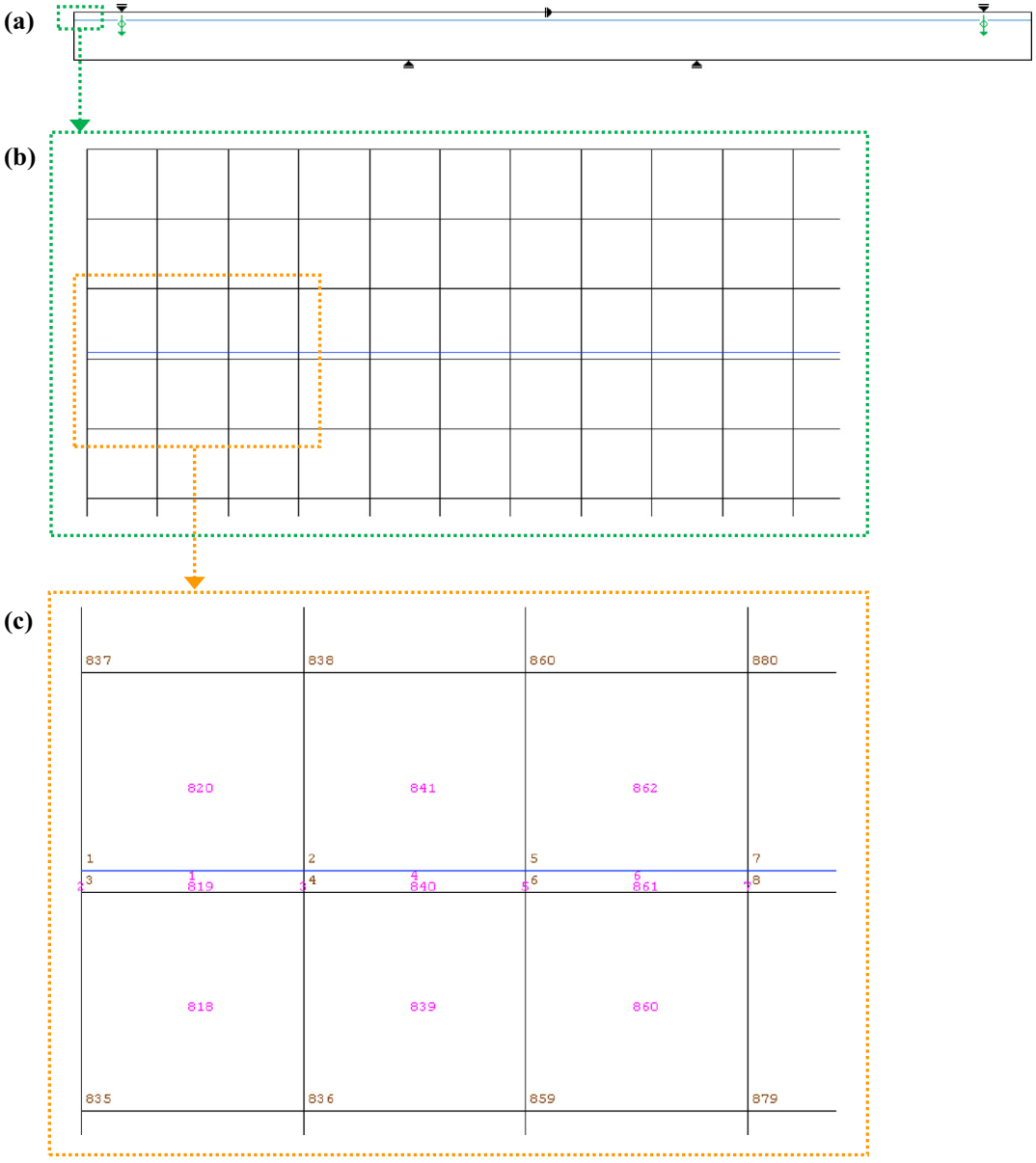

Fig. 18. Finite element mesh for beam test: (a) major elements, (b) detail of the total mesh, (c) multi-detailed mesh with element and node numbers.

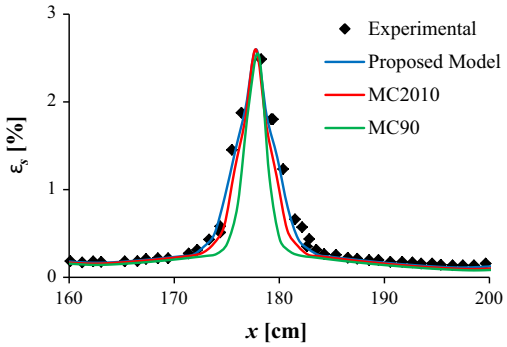

Fig. 19. Beam test [16]: steel strain.

than the 'Proposed Model'. The base model ('MC90') results in a very short yielding steel length.

The slip curve is a simple representation of the integral of steel strain curve, so conclusions about the performance of the slip curves are similar to those inferred for steel strain. The slip in the 'Proposed Model' was lower than the 'Experimental' data collected during the test devised by Shima et al., but higher than the 'Experimental' data collected by Bigaj and, in both tests, higher than the 'MC2010' model. It was still evident, however, that small differences in the curve of strain may cause large differences in the slip curve and consequently a specific steel strain in a crack could correspond to very different slips.

3.3. Bending tests in beams

The third comparison selected was a pure bending test of a beam, as performed by Kenel et al. [16]. In the elements subjected to the bending, the concrete near the rebar is in tension, and therefore it was expected that the bond–slip relationship would be much more similar to the ties test than the pull-out tests.

3.3.1. Test set-up

Fig. 17 shows the test set-up and the dimensions of the tested beam. The reinforcement ratio was 0.16%, which means that the bond near the cracks is important for estimating the ductility and the deflection of this beam.

3.3.2. Numeric model

Fig. 18 shows the major elements of the finite element mesh, the supports and the loading required to simulate this test. Once again, with the exception of the values for the mechanical properties of materials, which were defined as reported by the authors of the test [16], all parameters were the same as those assumed in Section 3.1.2.

3.3.3. Results

Fig. 19 compares the steel strains near a crack in the mid-span of the beam. As observed in the previous examples, the effect of steel strain on bond is essential to achieve realistic results. The base model ('MC90') showed a plastic zone with a length 45% lower than the 'Experimental' data, but the other two models exhibited good approximation to the 'Experimental' data, especially the 'Proposed Model'.

The position of numerical cracks was slightly adjusted in Fig. 19 to match the position of experimental cracks, because it is impossible to predict the exact location of cracks in a heterogeneous material such as concrete. Note however that the crack spacing determined in the numerical model is similar to the crack spacing obtained in the experimental test.

Fig. 20 shows the crack patterns for this beam test. Between supports, where bending is constant, the crack spacing exhibited in the numerical model is quite similar to the experimental test. On the other hand, near the supports, the numerical model shows more cracks than the experimental test.

4. Discussion and conclusions

4.1. Discussion

The bond element proposed in this paper allows to simulate the bond–slip relationship including (or not) the effect of steel strain. Compared with other formulations in the literature, mentioned in Chapter 1, the element developed has the advantage of estimating realistic values for slip and steel strain from the strains of the element itself; therefore it does not use non-local analysis or obtain information from the other elements.

This element was included with success in several numerical examples to simulate real tests in different concrete stress states. In all examples this element worked correctly and provided more realistic results than the base model, where the effect of steel strain in the bond–slip relationship is not taken into account. This suggests that the developed element could be useful in more complex analysis of reinforced concrete structures.

The results of several developed numerical models indicated that the reduction function $f(\varepsilon_s)$ (or similar) is essential to achieve realistic results for steel strains and concrete strains, after the yielding of rebars. This is consistent with the literature mentioned in Section 1, which observed the importance of steel strain in the bond–slip relationship. It is also questionable if, in the totally tension elements, will not be the steel strain to control the bond stress instead of slip.

The function proposed for $f(\varepsilon_s)$ provided numerical results consistent with experimental data. For current high ductility rebars, like ductility classes C and D in MC2010 [2], the function proposed is quite similar to the more complex function $\Omega_y(\varepsilon_s)$ of MC2010 [2]; however, the function $f(\varepsilon_s)$ has minimum values higher than the minimum values of the function $\Omega_y(\varepsilon_s)$. Although the function RP of Ruiz et al. [9] has faster decay, like two previous functions ($f(\varepsilon_s)$ and $\Omega_y(\varepsilon_s)$), it appears to be a suitable function for simulating the bond reduction. On the other hand, according to the analysis illustrated in Fig. 4, the function proposed by Wu and Gilbert [10] does not seem to be an appropriate function for this purpose.

The function $f(\varepsilon_s)$ was calibrated with tests in ties, that is, situations where the concrete is in pure tension, so it shows some

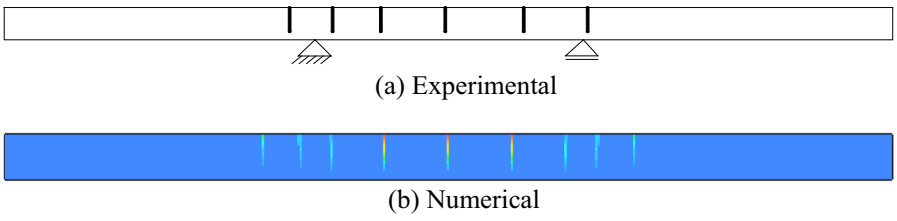

Fig. 20. Crack pattern: numerical vs experimental.

cracking. Thus, it was expected that the numerical results obtained in pure tension and bending would be closer to the experimental data than in cases where the concrete was in compression, as indeed it turned out. Note that in a situation of compressed concrete, apart from the concrete remaining intact, there is also a diametrical compression stress, which increases the bond. The function $\Omega_y(\varepsilon_s)$ seems to be more suitable for the situation of compressed concrete.

Taking into account that bond–slip is influenced by steel strain, as indicated in this paper and in the literature, it would be interesting to extend this knowledge to other types of rebar. Thus future research on pre-stress rebars and fibre-reinforced polymers (FRP) is suggested. Note that in these materials there is no distinct yield plateau, but materials can reach high strains which could crack the concrete and reduce the bond stress.

4.2. Conclusions

The influence of steel strain in bond–slip relationship was demonstrated in recent literature, mainly for steel strains after the yield. To include this knowledge in FE modelling, a new bond element was developed. This element permitted inclusion of steel strain effect in bond–slip relationship without requiring any type of non-local analysis.

The comparison between experimental and numerical results allowed precise simulation of the response of bond, slip and steel strain near cracks. It also showed the need to use this element to achieve good results and the relevance of steel strain effect in bond–slip relationship, especially in tension elements.

For this reason the bond element and the reduction function $f(\varepsilon_s)$ proposed are essential in the following problems: crack spacing, minimum reinforcement, tension stiffening, rotation capacity, ductility and deflection of cracked reinforced concrete structures.

Acknowledgements

The first author would like to express sincere appreciation and gratitude to the European Social Fund (ESF) and the Portuguese Foundation for Science and Technology (FCT) for the support received under Grant Number SFRH/BD/30004/2006. The authors also thank the FCT for support of the LABEST research unit (Laboratory for the Concrete Technology and Structural Behaviour).

References

[1] fib – Bulletin 10 – Bond of Reinforcement in Concrete. International federation for structural concrete (fib). Lausanne, Switzerland; 2000.
[2] fib – Bulletin 55 – Model Code 2010 – First Complete Draft, Volume 1. International federation for structural concrete (fib). Lausanne, Switzerland; 2010.
[3] Shima H, Chou L-L, Okamura H. Micro and Macro models for bond in reinforced concrete. J Faculty Eng Univ Tokyo Ser B 1987;39(2):133–94.
[4] Marti P et al. Tension Chord model for structural concrete. Struct Eng Int: J Int Assoc Bridge Struct Eng (IABSE) 1998;8(4):287–98.
[5] Mayer U, Eligehausen R. Bond behaviour of ribbed bars at inelastic steel strains. In: Proceedings of 2nd international Ph.D. symposium in civil engineering. Budapest; 1998.
[6] Lundgren K, Gylltoft K. A model for the bond between concrete and reinforcement. Mag Concrete Res 2000;52(1):53–63.
[7] Ožbolt J, Lettow S, Kožar I. Discrete bond element for 3D finite element analysis of reinforced concrete structures. In: Proceedings of bond in concrete 2002: from research to standards (3rd international symposium). Budapest, Hungary; 2002.
[8] Lowes LN, Moehle JP, Govindjee S. Concrete-steel bond model for use in finite element modeling of reinforced concrete structures. ACI Struct J 2004;101(4):501–11.
[9] Ruiz MF, Muttoni A, Gambarova PG. Analytical modeling of the pre- and post-yield behavior of bond in reinforced concrete. J Struct Eng-ASCE 2007;133(10):1364–72.
[10] Wu HQ, Gilbert RI. Modeling short-term tension stiffening in reinforced concrete prisms using a continuum-based finite element model. Eng Struct 2009;31(10):2380–91.
[11] CEB, CEB-FIP model code 1990: design code. London: Thomas Telford Ltd.; 1993.
[12] Lee SC, Cho JY, Vecchio FJ. Model for post-yield tension stiffening and rebar rupture in concrete members. Eng Struct 2011;33(5):1723–33.
[13] Manie J, Kikstra WP. DIANA-9.42 user's manual – material library. Delft: TNO DIANA BV; 2010.
[14] Rots JG, Blaauwendraad J. Crack models for concrete: discrete or smeared? Fixed, multi-directional or rotating? Heron 1989;34(1):3–59.
[15] Bigaj AJ. Structural dependence of rotation capacity of plastic hinges in RC beams and slabs. PhD thesis. Poland: Warsaw University of Technology; 1999
[16] Kenel A et al. Reinforcing steel strains measured by Bragg grating sensors. J Mater Civ Eng 2005;17(4):423–31.